Spectrochimica Acta Part A: Molecular and Biomolecular Spectroscopy 324 (2025) 124978

Contents lists available at ScienceDirect

Spectrochimica Acta Part A:
Molecular and Biomolecular Spectroscopy

journal homepage: www.journals.elsevier.com/spectrochimica-acta-part-a-molecular-and-biomolecular-spectroscopy

# Exploring the conformational landscape through rotational spectroscopy and computational modelling: The tunneling dynamics in 2,6-diethylphenol

Marcos Juanes [a,1], Lorenzo Paoloni [b,1], Wenqin Li [a], Antonio Picón [b,c], Sonia Melandri [d], Assimo Maris [d], Alberto Lesarri [a,*], Luca Evangelisti [d,*]

[a] Departamento de Química Física y Química Inorgánica, Facultad de Ciencias—I.U. CINQUIMA, Universidad de Valladolid, Paseo de Belén 7, 47011 Valladolid, Spain
[b] Departamento de Química, Universidad Autónoma de Madrid, 28049, Madrid, Spain
[c] Condensed Matter Physics Center (IFIMAC), Universidad Autónoma de Madrid, 28049, Madrid, Spain
[d] Department of Chemistry "G. Ciamician" - University of Bologna, Via F. Selmi 2, Bologna, Italy

## HIGHLIGHTS

- 2,6-diethylphenol measured in a jet supersonic expansion using rotational spectroscopy.
- The rotational constants for two conformers and $^{13}C$ isotopologues have been obtained.
- The structure of 2,6-diethylphenol is determined by DFT calculations and validated by Kraitchman's equation.
- The large amplitude motion of hydroxyl group has been determined around 100 MHz.

## GRAPHICAL ABSTRACT

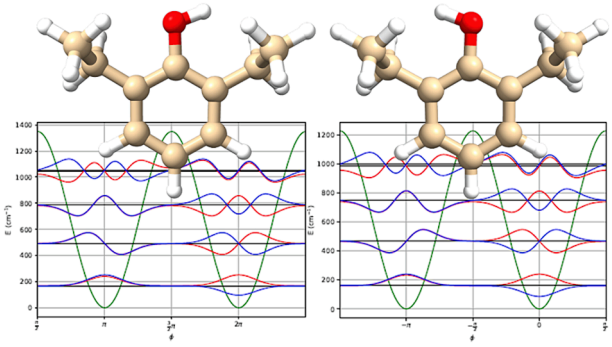

## ARTICLE INFO

*Keywords:*
Molecular structure
Large Amplitude Motions
Rotational spectroscopy
Supersonic jet spectroscopy

## ABSTRACT

Phenol and some of its derivatives exhibit interesting tunneling motions consisting of two groups of transitions separated by a few hundred MHz. Recently, one of its derivatives, 2,6-di-*tert*-butylphenol, has shown additional hyperfine tunneling components, the origin of which remains unclear. In this work, another member of the family, 2,6-diethylphenol, has been investigated through its rotational spectrum. The jet-cooled broadband chirped-pulse Fourier transform microwave spectra in the 2–8 GHz frequency region revealed the presence of two conformers. The comparison with the equilibrium structure obtained by computational calculations at the B3LYP-D3(BJ)/Def2-TZVP level validates the structural determination and the orientation of the lateral ethyl groups. Additional observation of all the singly-substituted $^{13}C$ isotopologues for the most stable ones allowed the determination of the substitution structure by means of the Kraitchman equations. Both conformers exhibited tunneling that was reproduced using an advanced 1D model, which provides an estimate of the barrier height for both conformers.

* Corresponding authors.
*E-mail addresses:* alberto.lesarri@uva.es (A. Lesarri), luca.evangelisti6@unibo.it (L. Evangelisti).
[1] These authors contributed equally.

https://doi.org/10.1016/j.saa.2024.124978
Received 16 June 2024; Received in revised form 10 August 2024; Accepted 12 August 2024
Available online 13 August 2024

## 1. Introduction

Phenol is an organic compound characterized by an aromatic ring to which a hydroxyl group is attached. Several spectroscopic techniques have been used to investigate this compound [1–5]. Among the various techniques employed is microwave spectroscopy, which can characterize both the structure and the internal motions of the molecule [6–10]. Microwave spectroscopic investigation has revealed a tunneling splitting of the $\mu_b$-type transitions in the vibrational ground state due to the internal rotation of the hydroxyl group. This molecule has been historically well-utilized, but a fundamental property lies in the fact that it serves as a backbone for a class of antioxidant molecules. These belong to the category of radical scavengers as they capture free radicals, delaying degradation processes by forming more stable radicals.

In this context, a series of molecules derived from phenol have been recently studied [11–14] to evaluate their chemical-physical properties, namely 2-*tert*-butylphenol (TBP) and 2,6-di-*tert*-butylphenol (26BP). Analyzing their structural properties is crucial to understanding their mechanism of action, and rotational spectroscopy has always been one of the most accurate tools for obtaining detailed information on structure, large-amplitude motions, and relative abundance of different conformations [15]. For 26BP, the situation is quite complex [13]. 26BP, in addition to the phenolic mainframe, has two *tert*-butyl groups in the *ortho* positions relative to the hydroxyl group. The molecular structure allows for only one possible conformer, but the spectrum presents phenomena not yet fully understood. As with phenol or some symmetrically substituted derived molecules, the spectrum shows the effects of a primary motion due to the equivalent positions of the hydroxyl group. This torsional separation, which is about 112 MHz in phenol, becomes 180 MHz in 26BP. In addition, each rotational transition presents a fine structure characterized by 3 components with relative intensities approximately 0.7:1:0.2 over a range of about 1 MHz. While a simplistic model has been proposed to reproduce the primary splitting, there is not yet sufficient information to understand the origin of the fine structure.

In contrast, the analysis for TBP is not particularly challenging [14]. TBP differs from 26BP by the absence of one *tert*-butyl group, which causes a decrease in molecular symmetry, preventing the observation of tunneling due to the hydroxyl group. Consequently, a very detailed structural analysis of TBP has been obtained. In this study, another phenol derivative was investigated in which the substituents in the *ortho* positions relative to the hydroxyl group are now ethyl groups, namely 2,6-diethylphenol (26EP, see Fig. 1). This increases the flexibility of the linear chains, as these groups can be oriented in various positions both relative to the hydroxyl group and to the plane of the ring. Despite the increased complexity, it guarantees the possibility of maintaining a symmetry that allows the observation of large-amplitude motions. Surprisingly, this molecule seems unexplored by any spectroscopic technique, at least in the isolated phase. Therefore, we report the analysis of 26EP by applying modern computational calculations and chirped-pulse Fourier Transform microwave (CP-FTMW) spectroscopy in order to: i) determine the conformational stability of 26EP; ii) accurately determine the molecular structure; iii) investigate the observed large-amplitude motions to obtain more information that can be correlated with possible fine components in the spectrum.

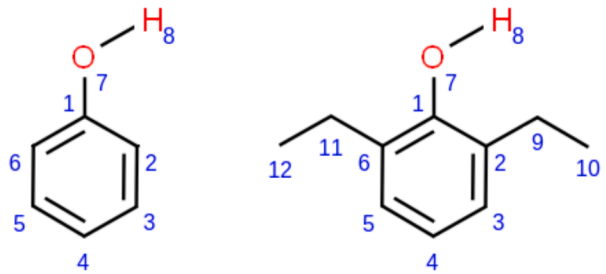


**Fig. 1.** Sketch and numbering of the atoms of phenol and 2,6-diethylphenol.

## 2. Quantum chemical calculations

26EP is a molecule derived from phenol, whose conformation fundamentally depends on 3 dihedral angles. Besides the dihedral angle that describes the orientation of the hydroxyl group relative to the plane of the aromatic ring (C6C1O7H8), there are two other dihedral angles that describe the positions of the ethylene substituents near the hydroxyl group (specifically C12C11C6C1, C10C9C2C1). Considering the relatively low number of variables, a systematic search was chosen to investigate the conformational space of 26EP [16]. In this case, if we consider $A$ as the increment of the torsional angle, $R$ as the allowed rotation range, and $T$ as the number of rotatable bonds, then the total number of possible conformers to be examined becomes:

$$\Pi_{i=1,T}(R_i/A_i)$$

Pure symmetry considerations allow for a depth-first search with tree pruning during the conformational search.

The GAUSSIAN16 suite of programs [17] was used for the geometric optimization of conformers derived from the systematic search. Among the various available methods, B3LYP was chosen and empirical dispersion terms were added using the Grimme D3 method with the Becke-Johnson damping function (D3(BJ)). Additionally, the split valence Weigend & Ahlrichs – triple ξ basis set was chosen [18–20]. This level of calculation has proven to be effective in analogous systems, providing a good compromise between computation time/hardware resources required and the results obtained [21,22]. A total of 5 distinct conformers were obtained, whose molecular structures and calculated spectroscopic values are reported in Table 1.

Harmonic vibrational frequency calculations were used to verify if the optimized structure was a minimum and to obtain the relative zero-point corrected energies. In all species, the hydroxyl group is almost coplanar with the aromatic ring, oriented towards either C2 or C6. The difference lies in the orientation of the ethyl chains, which can be nearly coplanar or perpendicular to the phenyl group. If both chains are out of the plane, they can either lie on the same side of the ring (conformer I) or on opposite sides (conformer II). If only one chain is out of the plane, the hydroxyl group can be oriented towards the coplanar ethyl chain (conformer III) or away from it (conformer IV). Finally, if both chains are in-plane, the system exhibits $C_s$ symmetry (conformer V).

Conformers I and II are predicted to be the most stable, with very similar energies, followed by conformers III and IV, which are about 200–300 $cm^{-1}$ higher in energy. Conformer V is the least stable, at 475 $cm^{-1}$. Due to symmetry, conformer V has two equivalent forms, while conformers I, II, III, and IV have each four equivalent forms. It is worth noting that a symmetric interconversion pathway involving only the internal rotation of the hydroxyl group, similar to that observed in phenol, is possible only for conformers I, II, and V.

## 3. Experimental

The sample of 26EP (CAS: 1006–59-3 and InChIKey: METWAQRCMRWDAW-UHFFFAOYSA-N) was analyzed using the broadband chirped-pulse Fourier transform microwave (CP-FTMW) spectrometer at the University of Valladolid, previously described [23]. The sample was loaded into a sample reservoir inserted into an inert gas line (a mix of argon and helium). This allowed for the recording of the rotational spectrum under supersonic jet expansion conditions, achieving rotational temperatures close to 1 K (estimated through simulation with SPCAT[23,24]). To obtain sufficient vapor pressure, the sample was heated to 358 K, while the backing pressure of the inert gas was 0.2 MPa. The gas mixture was pulsed into the chamber (with a final pressure of about 0.05 mPa) using a Parker General Valve – Series 9 pulsed valve (0.8 mm diameter), typically operating at 5 Hz. With each

molecular pulse, the sample was excited by a 4 μs chirped pulse produced by a fast arbitrary waveform generator (25 GS/s) and amplified by a 200 W amplifier in the 2–8 GHz range. A molecular transient emission was captured by a horn antenna, amplified by a low-noise amplifier, and sampled at 25 GS/s by a digital oscilloscope. The entire measurement sequence was repeated 8 times for each molecular pulse. The final time-domain spectrum comprised 520 k averages. Subsequently, the frequency-domain spectrum was obtained via Fourier transform using a Kaiser-Bessel apodization window. Typically, the uncertainty of the frequency measurements and resulting linewidths at full width at half-maximum were 20 kHz and 100 kHz, respectively.

## 4. Results

As already discussed, computational calculations predict 5 stable conformers and in principle, all of these could be observed during our experiment since the experimental spectrum recorded in the 2–8 GHz range displays very intense transitions. The initial analysis was based on the consideration that the conformers have more intense predicted $\mu_a$-type dipole moments. According to this consideration, a series of transitions showing tunneling splitting was observed. This splitting is similar to analogous phenol derivatives and originates from the large amplitude motion of the hydroxyl group. The splitting is approximately 200 MHz and separates the transitions into two distinct groups because the $\mu_a$-type transitions are torsionally interstate. Following this initial assignment, another similar pattern was observed in the remaining transitions, but with the splitting reduced to about 168 MHz. In this case, the spectrum belongs to the second predicted most stable conformer. Similar to the first case, the same motion of the hydroxyl group connects two equivalent structures and the $\mu_a$-type transitions are again torsionally interstate.

For each conformer, all transitions were fitted using Watson's *S*-reduced Hamiltonian in the $I^r$ representation [24], employing a semi-rigid rotor term ($H^R$) common to the two states and an additional two-state torsion-rotation coupled Hamiltonian, which yielded a specific torsional energy difference $\Delta E$ and a Coriolis coupling term $F_{ab}$, determined in the reduced-axis system proposed by Pickett [25]:

$$H = H^R + H^{int}$$

where:

$$H^{int} = \Delta E + F_{ab}(P_a P_b + P_b P_a)$$

and where $P_\alpha$ (with α can be *a* or *b*) represents the angular momentum operators. The results of the fitting procedure are summarized in Table 2.

For conformer I, the transition intensities are sufficiently strong to allow the observation of the spectra of $^{13}C$ isotopologues in natural abundance (about 1 % of the spectrum of the normal species). Therefore, a set of rotational constants for each isotopologue was observed and assigned as reported in the supplementary material.

**Table 2**
Experimental spectroscopic parameters of 26EP.

| | Conf I | Conf II |
|---|---|---|
| *A* / MHz | 1595.0160(32) | 1706.261(30) |
| *B* / MHz | 881.9135(22) | 847.6188(25) |
| *C* / MHz | 637.1510(20) | 618.6799(29) |
| $D_J$ / kHz | 0.090(50) | |
| $D_{JK}$ / kHz | −0.271(43) | |
| $D_K$ / kHz | 0.59(18) | |
| $d_1$ / Hz | 28(4) | |
| $\Delta E_{01}$ / MHz | 100.7327(46) | 84.4554(60) |
| $\lvert F_{ab} \rvert$ / MHz | 1.57(16) | 1.70(45) |
| $\sigma$ [a] / kHz | 9 | 5 |
| $N$ [b] | 141 | 57 |

[a] Standard deviation of the fit;
[b] Number of transitions included in the fit.

**Table 1**
Relative energy values and spectroscopic parameters of the five conformers of 26EP at the B3LYP-D3(BJ)/Def2-TZVP level of calculation.

| | Conf I | Conf II |
|---|---|---|
| | 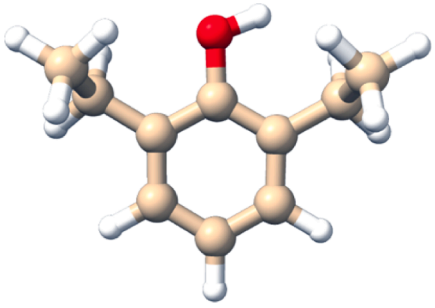 | 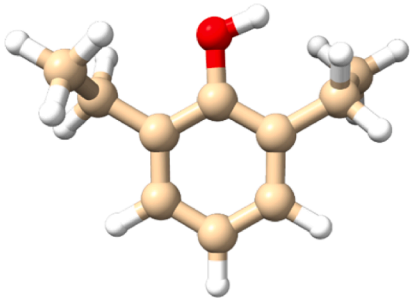 |
| *A*,*B*,*C*/MHz | 1603.6, 883.1, 638.8 | 1716.9, 848.7, 620.2 |
| $\mu_a$, $\mu_b$, $\mu_c$/D | −1.4, −0.3, −0.1 | 1.4, 0.3, 0.3 |
| $\Delta E$, $\Delta E_0$/cm$^{-1}$ | 0[a], 0[b] | 13, 4 |

| | Conf III | Conf IV | Conf V |
|---|---|---|---|
| | 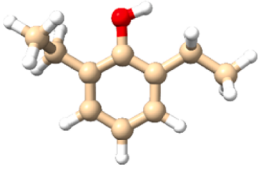 | 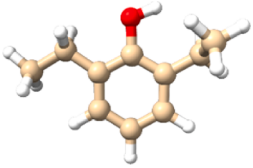 | 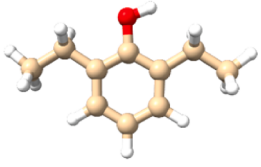 |
| *A*,*B*,*C*/MHz | 1937.4, 770.4, 584.3 | 1937.9, 768.7, 584.1 | 2220.0, 708.5, 544.2 |
| $\mu_a$, $\mu_b$, $\mu_c$/D | 1.5, 0.6, 0.0 | −1.3, −0.2, −0.1 | −1.4, −0.5, 0.0 |
| $\Delta E$, $\Delta E_0$/cm$^{-1}$ | 214, 203 | 263, 266 | 475, 472 |

[a] Absolute energy: −464.953616 hartrees.
[b] Absolute energy: −464.736482 hartrees.

## 5. Discussion

The assignments of the observed species to the different conformations are based on several discriminating factors. Only 3 of the 5 calculated species (I, II, and V) have symmetry that allows for the observation of a tunneling motion. Since species III and IV fundamentally lack symmetry elements, the observed spectra cannot belong to these species. The comparison of the experimentally determined rotational constants with those predicted by computational calculations leads to an unambiguous identification of the observed species belonging to conformers I and II. The discrepancy in values is less than 0.6 % for all constants. Additionally, the identified species are also the most stable calculated ones, which means that their population should be more abundant. Species V, besides having predicted rotational constants significantly different from the determined ones, also has higher energy compared to the others, making its population lower in the jet and therefore not observed.

We hypothesized that collisional mechanisms within the jet result in effective conformational relaxation into the global minimum, as empirically observed when the interconversion barrier between equilibrium minima is below $2kT$ (about 400 $cm^{-1}$) [26,27]. Support for this proposition stems from the discrepancy between the expected II/I population ratio of 0.94 according to a Boltzmann distribution and the lower experimental intensity ratio, approximately 0.27.

The experimental confirmation of the observed conformer I also comes from its experimental structure. As previously reported, the intensity of conformer I is sufficient to observe the spectrum of $^{13}C$ monosubstituted species in natural abundance. The inherently high resolution of microwave spectroscopy allows for the characterization of different rotational constants for each isotopologue. These are derived from the moments of inertia and thus from the three-dimensional spatial distribution of the atomic masses. From the experimental spectrum, all 10 individual $^{13}C$ isotopologues were identified, leading to the following conclusions:

1. The large amplitude motion of the hydroxyl group can be observed only if the molecule's symmetry is not perturbed by isotopic substitution. This condition holds true only at positions C1 and C4, where the internal motion persists in these rotational spectra.
2. For all other positions, isotopic substitution disrupts the symmetry, rendering the two positions of the hydroxyl group non-equivalent. In these cases, a distinct spectrum for each isotopologue is observed, similar to that of a rigid rotor perturbed only by centrifugal distortion effects. Due to the disappearance of the splitting, the relative intensities of the isotopologue spectra are higher than the hypothetical value (about 1 %) relative to the normal species spectrum.

Using the rotational constants obtained from the various isotopologues, different procedures can be employed to derive the experimental structure of the observed conformer. One widely used method is the solution of Kraitchman's equations [28]. A significant advantage of this method is that it does not require assuming a priori structure, and the positions of the various monosubstituted atoms relative to the Cartesian system of the normal species are generally easily derived [29,30]. In our case, we derived the positions of the various carbon atoms and compared them with the equilibrium structure obtained from B3LYP-D3 (BJ)/Def2-TZVP level calculations. There is a close correspondence between the experimental and calculated structures, confirming that the most stable conformer has the ethylene groups lying on the same side with respect to the aromatic ring. The results of Kraitchman's analysis are available in Table 3.

Interestingly, the only other observed structure for 26EP is through X-ray crystallography [31], where 26EP served as a ligand within GABAA receptors. In this case, the observed conformer is II, where the ethylene groups are in the *anti* position relative to each other. It should be noted that in a crystalline structure, the observed conformation strongly depends on the environment, and matrix effects due to crystal packing play a significant role in the conformational stability of the ligand.

## 6. Intramolecular dynamics

In order to reproduce the experimental tunneling splittings, we apply a numerical 1D approach to solve the rovibrational problem related to the hydroxyl internal rotation, i.e. a periodic intramolecular motion, with a periodicity that is affected by identities and positions of the eventual substituents of the phenyl ring.

The implementation is based on the early work of Meyer [32,33] and was already described (and applied) in refs. [34]. Briefly, the numerical solution of the 1D problem is determined by (i) the potential energies ($V(\tau)$) and (ii) the molecular geometries of the molecular system of interest at different values of the involved internal coordinate ($\tau$). These quantities are obtained theoretically with a relaxed scan along $\tau$, and then the 1D nuclear problem associated with $\tau$ is solved according to the following computational protocol:

1. By parsing the output of the relaxed scan (i) a 1D cut of the potential energy surface ($V(\tau)$) and (ii) the evolution of the molecular geometry are obtained;
2. Nuclear cartesian coordinates and potential energy of the molecular system are extracted, and the nuclear Cartesian coordinates are expressed in the Principal Axis System (PAS) through suitable rotations and translations. Then, the first derivative of all the nuclear Cartesian coordinates is calculated at each value of $\tau$ and employed to construct the $4 \times 4$ kinetic energy matrices (one for each value of the internal coordinate of interest), their determinants, and their inverses;
3. Finally, the data are employed to formulate a rovibrational Hamiltonian ($H_{vibrot}$) for the case $J$=0, and the associated rovibrational problem is solved as an eigenvalue problem, obtaining the energy levels and 1D wavefunctions.

Some of the peculiarities of the code employed to calculate the results reported and discussed in this communication must be mentioned:

1. In contrast with the old (but pioneering, at that time) codes of Meyer, the code used to carry out the calculations here reported automatically reads energies and molecular geometries from the output of a relaxed scan (the code is currently interfaced to Gaussian, but can be easily interfaced to other quantum chemical packages with the simple addition of a function to parse a different output format);
2. In order to obtain accurate solutions for the vibrorotational problem, the convergence parameters employed during the optimizations are very important. Specifically, both energies and nuclear coordinates of the molecular system should be smooth functions (with the proper symmetries) of the intramolecular coordinate employed to perform

**Table 3**
Experimental substitution coordinates and theoretical equilibrium coordinates of the observed $^{13}C$ isotopologues of conformer I − 26EP.

| | *a* (Å) | | *b* (Å) | | *c* (Å) | |
|---|---|---|---|---|---|---|
| | $\|r_s\|$ | $r_e$ | $\|r_s\|$ | $r_e$ | $\|r_s\|$ | $r_e$ |
| C1 | 0.07*i*(8) | 0.007 | 0.33(2) | −0.354 | 0.35(1) | −0.377 |
| C2 | 1.213(3) | −1.220 | 0.28(1) | 0.301 | 0.24(1) | −0.241 |
| C3 | 1.198(4) | −1.208 | 1.676(3) | 1.664 | 0.06(9) | 0.049 |
| C4 | 0.09(13) | −0.016 | 2.360(5) | 2.354 | 0.18(7) | 0.205 |
| C5 | 1.209(4) | 1.187 | 1.669(3) | 1.676 | 0.06(9) | 0.065 |
| C6 | 1.217(3) | 1.225 | 0.30(1) | 0.317 | 0.24(1) | −0.229 |
| C9 | 2.527(1) | −2.523 | 0.43(1) | −0.447 | 0.37(1) | −0.360 |
| C10 | 2.880(2) | −2.887 | 1.235(5) | −1.227 | 0.905(6) | 0.910 |
| C11 | 2.528(1) | 2.529 | 0.42(1) | −0.423 | 0.37(1) | −0.354 |
| C12 | 2.868(1) | 2.878 | 1.233(4) | −1.227 | 0.903(5) | 0.903 |

the relaxed scan. With the default optimization algorithm (and the default thresholds) of the Gaussian suite, the energy is usually a smooth function, but this is often not the case for some of the nuclear coordinates. To solve this problem, one can (i) decrease the threshold employed to test the convergence of the optimization procedure for the relaxed scan (this solution is computationally expensive) or (ii) refine the results through a series of fits to the elements of a Fourier series, using this procedure also to enforce the proper symmetry to the functions of interest. In the code employed to produce the results reported here, the second solution is available.

3. To formulate the Hamiltonian for the case $J$=0, the same basis suggested in the early work of Meyer was used, with an odd number of points in the mesh grid.

To validate the numerical approach mentioned above, we applied the procedure to the hydroxyl torsion ($\tau$) in the phenol molecule (for which experimental data are available in the literature). Then, the same approach was employed to simulate splittings, barrier heights, and energy levels of the 2 observed conformers of 26EP (I and II). All the relaxed scan calculations reported in what follows were performed at the B3LYP- D3(BJ)/Def2-TZVP level of theory, using a step $\Delta\tau = 1°$.

### 6.1. Phenol: Validation of the model

In the case of phenol, extremely tight convergence criteria were used for the relaxed scan calculation. The convergence thresholds for the geometry optimizations were root mean square (RMS) values of $1{\cdot}10^{-6}$ hartree/bohr and $4{\cdot}10^{-6}$ bohr and maximum values of $2{\cdot}10^{-6}$ hartree/bohr and $6{\cdot}10^{-6}$ bohr on forces and displacements, respectively. The resulting $V(\tau)$ is symmetric with two planar minima ($\tau = 0°$,180°) and identical barriers ($\tau$=±90°) as shown in Fig. 2. Taking into account its symmetry, $V(\tau)$ was fitted with the even cosine terms of a Fourier series and the vibrorotational analysis provided the results summarized in Table 4 while Fig. 2 provides a graphical representation of the results. It is well-known that energy levels are greatly affected by the height of the energy barrier, and for this reason different scaling factors were applied to modulate the barrier height (i.e. the actual barrier height is expressed as $V_{act} = k{\cdot}\Delta V_{calc}$).

A comparison between calculated and experimental results (Table 4) suggests that DFT calculations overestimate the barrier height of about 150–200 $cm^{-1}$: to reproduce the energy splitting between symmetric and antisymmetric pairs of sublevels (see Table 4), a scaling factor $k$ = 0.86 seems to be almost optimal, but with such a scaling factor the calculated splitting between successive symmetric eigenfunctions (bottom of Table 4, the corresponding wavefunctions are the red ones shown in Fig. 2) are too small with respect to the experimental energy differences reported in literature [2,35]. In order to optimize the splittings between successive symmetric eigenfunctions, we can increase the scaling factors to 0.91 (see Table4).

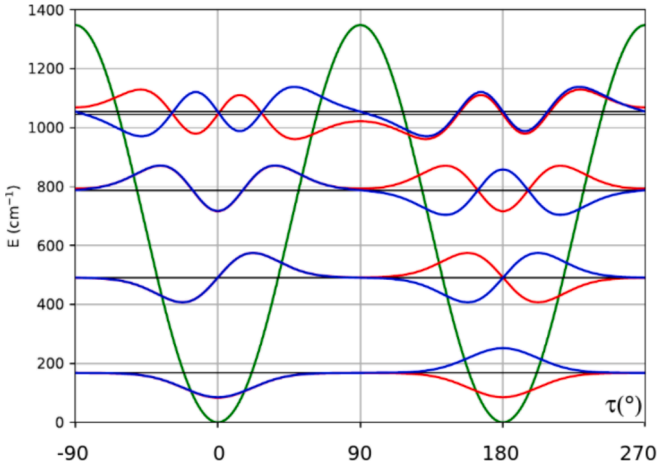


**Fig. 2.** 1D-PES, energy levels and wavefunctions related to the intramolecular OH torsion of the phenol molecule. The values can be found in the ESI† and in the AMSActa.

The model takes into account all the structural relaxations with the proper symmetry, but the accuracy is limited by the level of theory employed (B3LYP-D3(BJ)/Def2-TZVP), and therefore the existence of a discrepancy between the optimal scaling factor suggested by the calculated energy splittings between symmetric and antisymmetric pairs of sublevels on one hand and the optimal scaling factor suggested by the calculated splittings between successive symmetric eigenfunctions on the other hand is not surprising. The factor behind this discrepancy is probably a slight inaccuracy in the energy barrier thickness calculated at B3LYP-D3(BJ)/Def-2TZVP level of theory. However, despite structure relaxations having been taken into account as functions of the OH torsion, it cannot be excluded that their effect is underestimated.

### 6.2. 26EP

Due to the out-of-plane orientation of the ethyl chains, conformers I and II of 26EP are less symmetric than the phenol molecule. For conformer II, the molecular structures which correspond to the energy minimum (maximum) have a dihedral angle $\tau$ = 3.7°/183.7°(97.7°/277.7°), as shown in Fig. 3. The two barriers have the same shape and the same height, but they are not symmetric (i.e. the two sides of a single barrier do not have the same slope). In other words V($\tau$) is periodic and has no mirror-imaged symmetry about the energy maximum. Taking into account its symmetry, $V(\tau)$ can be fitted with the even sine and the even cosine terms of a Fourier series.

In the case of 26EP, geometry optimizations were carried out using looser convergence criteria with respect to those used for phenol, that is the default convergence criteria of G16 (RMS values of $3{\cdot}10^{-4}$ hartree/bohr and $1.2{\cdot}10^{-3}$ bohr and maximum values of $4.5{\cdot}10^{-4}$ hartree/bohr and $1.8{\cdot}10^{-3}$ bohr on forces and displacements, respectively), in order to decrease the computational cost of the calculation. With this choice for the convergence thresholds, a subsequent refinement of the optimized geometries is needed to achieve good quality results for the numerical calculation of the derivatives of the nuclear positions. This refinement was performed with an automatic Fourier series fit of each of the cartesian coordinates obtained from the relaxed scan. In this manner, it is possible to avoid spurious oscillations (due to the high tolerance of the convergence threshold) for the numerical values of the calculated nuclear positions and therefore to construct an accurate $H_{vibrot}$ Hamiltonian matrix for the case $J$=0.

The obtained energy levels are reported in Table 5, while the corresponding wavefunctions are shown in Fig. 3. A comparison with the experimental value of the energy splitting between the symmetric and the antisymmetric sublevels suggests that the calculated energy barriers are higher than the real ones of about 300 $cm^{-1}$. In order to reproduce the experimental energy splitting, a scaling factor of 0.72 was employed (see Table 5).

In the case of conformer I, the hydroxyl rotation leads to two equivalent minima lying at $\tau = 6.45°/173.55°$ and two non-equivalent maxima lying at $\tau$=±90° (see Fig. 3). Taking into account its symmetry, $V(\tau)$ can be fitted with the even cosine and the odd sine terms of a Fourier series.

The obtained energy levels are reported in Table 5, while the corresponding wavefunctions are shown in Fig. 3, on the right.

Also in this case, the calculated energy barrier heights lead to a calculated splitting between the first symmetric and antisymmetric sublevels which is too small compared to the experimental value and the same $V(\tau)$ scaling factor $k = 0.72$ is necessary to reproduce the observed splitting.

The $k$ value obtained for 26EP is 0.72. However, this result is limited by the lack of experimental information, which is confined to the

**Table 4**
Torsional barriers ($B$), vibrational energy levels ($v$) and transitions ($\Delta v$) associated with the hydroxyl internal rotation of phenol calculated for different scaling values ($k$) of the potential energy function. The 1D internal rotation problem was solved numerically with a code written by the authors and mentioned in the text.

| *Parameters* | *Theoretical values* | | | | *Experimental values* | |
|---|---|---|---|---|---|---|
| $k$ | 1 | 0.91 | 0.88 | 0.86 | | |
| $B/cm^{-1}$ | 1348.49 | 1227.12 | 1186.67 | 1159.70 | | |
| $v = 0^+/cm^{-1}$ | 167.82 | 159.82 | 157.07 | 155.21 | | |
| $v = 1^+/cm^{-1}$ | 491.13 | 467.01 | 458.70 | 453.08 | | |
| $v = 2^+/cm^{-1}$ | 786.97 | 746.06 | 731.92 | 722.34 | | |
| $v = 3^+/cm^{-1}$ | 1045.10 | 984.40 | 963.24 | 948.85 | | |
| $\Delta v(0^+ \Leftrightarrow 0^-)/cm^{-1}$ | 0.00067 | 0.00128 | 0.00159 | 0.00185 | 0.0018679[8] | 0.0019[35] |
| $\Delta v(1^+ \Leftrightarrow 1^-)/cm^{-1}$ | 0.035 | 0.063 | 0.077 | 0.088 | 0.089629[8] | 0.0896[35] |
| $\Delta v(2^+ \Leftrightarrow 2^-)/cm^{-1}$ | 0.79 | 1.33 | 1.58 | 1.78 | | 1.77[35] |
| $\Delta v(3^+ \Leftrightarrow 3^-)/cm^{-1}$ | 9.44 | 14.28 | 16.36 | 17.90 | | |
| $\Delta v(0^+ \Leftrightarrow 1^+)/cm^{-1}$ | 323.31 | 307.19 | 301.63 | 297.87 | 309.0[2] | 309.17[35] |
| $\Delta v(1^+ \Leftrightarrow 2^+)/cm^{-1}$ | 295.84 | 279.05 | 273.22 | 269.26 | 275.4[2] | 275.70[35] |
| $\Delta v(2^+ \Leftrightarrow 3^+)/cm^{-1}$ | 258.13 | 238.34 | 231.32 | 226.51 | 236.8[2] | |

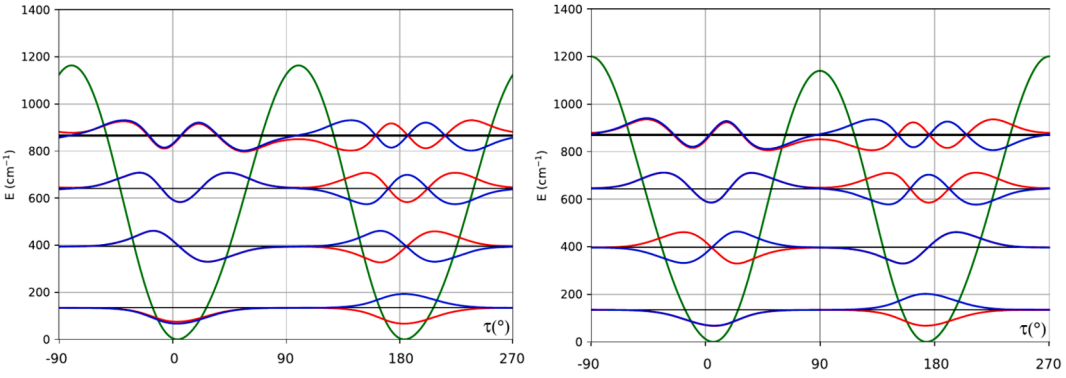


**Fig. 3.** On the left, 1D-PES, energy levels and wavefunctions related to the intramolecular OH torsion of 26EP – conformer II. On the right side, 1D-PES, energy levels and wavefunctions related to the intramolecular OH torsion of 26EP – conformer I. The values can be found in the ESI† and in the AMSActa.

**Table 5**
Torsional barriers ($B$), vibrational energy levels ($v$) and transitions ($\Delta v$) associated with the hydroxyl internal rotation of the two conformers of 26EP calculated for different scaling values ($k$) of the potential energy function.

| *Parameters* | Conf. I | | | Conf. II | | |
|---|---|---|---|---|---|---|
| $k$ | 1 | 0.91 | 0.72 | 1 | 0.91 | 0.72 |
| $B/cm^{-1}$ | 1140.05 | 1037.45 | 820.84 | 1163.65 | 1058.92 | 837.83 |
| | 1200.61 | 1092.55 | 864.44 | | | |
| $v = 0^+/cm^{-1}$ | 136.67 | 128.32 | 113.78 | 134.11 | 127.76 | 113.25 |
| $v = 1^+/cm^{-1}$ | 396.75 | 377.7 | 333.86 | 394.31 | 375.35 | 331.84 |
| $v = 2^+/cm^{-1}$ | 644.22 | 611.82 | 536.69 | 640.86 | 608.66 | 534.03 |
| $v = 3^+/cm^{-1}$ | 868.5 | 820.12 | 705.42 | 863.89 | 815.93 | 702.18 |
| $\Delta v(0^+ \Leftrightarrow 0^-)/cm^{-1}$* | 0.00054 | 0.00100 | 0.00414 | 0.00031 | 0.00061 | 0.00278 |
| $\Delta v(1^+ \Leftrightarrow 1^-)/cm^{-1}$ | 0.021 | 0.037 | 0.139 | 0.015 | 0.028 | 0.113 |
| $\Delta v(2^+ \Leftrightarrow 2^-)/cm^{-1}$ | 0.41 | 0.70 | 2.26 | 0.35 | 0.61 | 2.06 |
| $\Delta v(3^+ \Leftrightarrow 3^-)/cm^{-1}$ | 5.07 | 7.94 | 19.93 | 4.61 | 7.33 | 18.97 |
| $\Delta v(0^+ \Leftrightarrow 1^+)/cm^{-1}$ | 262.08 | 249.34 | 220.08 | 260.20 | 247.59 | 218.59 |
| $\Delta v(1^+ \Leftrightarrow 2^+)/cm^{-1}$ | 247.47 | 234.16 | 202.83 | 246.55 | 233.31 | 202.19 |
| $\Delta v(2^+ \Leftrightarrow 3^+)/cm^{-1}$ | 224.28 | 208.30 | 167.73 | 223.03 | 207.27 | 168.15 |

* Experimental values of $\Delta v(0^+ \Leftrightarrow 0^-)$ are 0.00336 and 0.00282 $cm^{-1}$ for conformers I and II, respectively (see Table 2).

splitting between the first two sublevels. For phenol, the inversion splittings can be satisfactorily reproduced with $k = 0.86$, though a slightly higher value of $k = 0.91$ better reproduces the $\Delta v$ energy values. The phenol results suggest that the model applied to the splittings tends to overcorrect the energy barrier. Therefore, for 26EP, we estimate a k factor of 0.8, corresponding to energy barriers of 912 $cm^{-1}$ and 960 $cm^{-1}$ for conformer I, and 945 $cm^{-1}$ for conformer II. However, we anticipate further verification of our findings as more experimental data become available.

## 7. Conclusions

In this work, the conformational behaviour of 2,6-diethylphenol (26EP) was studied using broadband FTMW spectroscopy. Out of the five conformers hypothesized by computational calculations, two were observed experimentally. These conformers have the ethyl groups in the gauche position and differ in the fact that, in the more stable conformer, they are on the same side of the plane, while in the second conformer, they are in opposite directions in the plane. For the more stable conformer, it was also possible to validate the structure through isotopic substitution of the $^{13}C$ atoms. Both conformers have sufficient symmetry for the hydroxyl group to occupy equivalent positions. This allows for

the observation of a tunneling phenomenon in the spectrum similar to that observed in phenol. This tunneling motion was described using a 1D model, which was validated against the phenol case and provides an estimate of the barrier height for both conformers.

## CRediT authorship contribution statement

**Marcos Juanes:** Validation, Investigation, Data curation, Writing – review & editing. **Lorenzo Paoloni:** Methodology, Data curation, Validation, Formal analysis, Visualization, Writing – review & editing. **Wenqin Li:** Validation, Investigation, Data curation, Writing – review & editing. **Antonio Picón:** Data curation, Writing – review & editing. **Sonia Melandri:** Methodology, Validation, Data curation, Writing – review & editing. **Assimo Maris:** Conceptualization, Methodology, Validation, Formal analysis, Data curation, Writing – review & editing. **Alberto Lesarri:** Conceptualization, Methodology, Validation, Formal analysis, Resources, Data curation, Writing – review & editing, Funding acquisition. **Luca Evangelisti:** Conceptualization, Methodology, Validation, Formal analysis, Resources, Data curation, Writing – original draft, Writing – review & editing, Funding acquisition.

## Declaration of competing interest

The authors declare that they have no known competing financial interests or personal relationships that could have appeared to influence the work reported in this paper.

## Data availability

We have shared our data in AMSActa: https://doi.org/10.6092/unibo/amsacta/7815.

## Acknowledgements

We acknowledge funding from the Spanish Ministerio de Ciencia e Innovación and the European Regional Development Fund (MICINN–ERDF, Grant No. PID2021-125015NBI00) and the Junta de Castilla y León (Grant No. INFRARED IR2021-UVa13). M. J. thanks the University of Valladolid for a "Margarita Salas" postdoc contract. W.L. thanks the China Scholarship Council for a research scholarship. We acknowledge the CINECA award under the ISCRA initiative, for the availability of high-performance computing resources and support. This work was supported by University of Bologna (RFO). L.P. and A.P. acknowledge the Spanish Ministry of Science, Innovation and Universities & the State Research Agency through grants refs. PID2021-126560NB-I00 and CNS2022-135803 (MCIU/AEI/FEDER, UE), and the "María de Maeztu" Programme for Units of Excellence in R&D (CEX2023-001316-M), and FASLIGHT network (RED2022-134391-T), and computer resources and assistance provided by Centro de Computación Científica de la Universidad Autónoma de Madrid and Barcelona Supercomputing Center (FI-2023-1-0035 and FI-2023-2-0012).

## Appendix A. Supplementary data

Supplementary data to this article can be found online at https://doi.org/10.1016/j.saa.2024.124978.

## References

[1] H.D. Bist, J.C. Brand, D.R. Williams, The vibrational spectrum and torsion of phenol, Journal of Molecular Spectroscopy 24 (1–4) (1967) 402–412.
[2] N.W. Larsen, F.M. Nicolaisen, Far-infrared gas spectra of phenol, 4-fluorophenol, thiophenol and some deuterated species: Barrier to internal rotation, Journal of Molecular Structure 22 (1) (1974) 29–43.
[3] H.W. Wilson, R.W. MacNamee, J.R. Durig, Raman spectra of gases: 24—Phenol, Journal of Raman Spectroscopy 11 (4) (1981) 252–255.
[4] S.J. Martinez III, J.C. Alfano, D.H. Levy, Rotationally resolved fluorescence excitation spectra of phenol and 4-ethylphenol in a supersonic jet, Journal of Molecular Spectroscopy 152 (1) (1992) 80–88.
[5] G. Berden, W.L. Meerts, M. Schmitt, K. Kleinermanns, High resolution UV spectroscopy of phenol and the hydrogen bonded phenol-water cluster, The Journal of Chemical Physics 104 (3) (1996) 972–982.
[6] T. Kojima, Potential barrier of phenol from its microwave spectrum, Journal of the Physical Society of Japan 15 (2) (1960) 284–287.
[7] N.W. Larsen, E. Mathier, A. Bauder, H.H. Günthard, Analysis of microwave and infrared transitions of phenol by rotation-internal rotation theory Phenol-OD, *Journal of Molecular Spectroscopy* 47 (2) (1973) 183–188.
[8] C. Tanjaroon, S.G. Kukolich, Measurements of the rotational spectra of phenol and 2-pyrone and computational studies of the H-bonded phenol− pyrone dimer, The Journal of Physical Chemistry A 113 (32) (2009) 9185–9192.
[9] L. Kolesniková, A.M. Daly, J.L. Alonso, B. Tercero, J. Cernicharo, The millimeter wave tunneling–rotational spectrum of phenol, Journal of Molecular Spectroscopy 289 (2013) 13–20.
[10] Z. Kisiel, Further rotational spectroscopy of phenol: Sextic centrifugal distortion and vibrational satellites, Journal of Molecular Spectroscopy 386 (2022) 111630.
[11] A. Lesarri, S.T. Shipman, J.L. Neill, G.G. Brown, R.D. Suenram, L. Kang, W. Caminati, B.H. Pate, Interplay of phenol and isopropyl isomerism in propofol from broadband chirped-pulse microwave spectroscopy, Journal of the American Chemical Society 132 (38) (2010) 13417–13424.
[12] W. Li, A. Maris, S. Melandri, A. Lesarri, L. Evangelisti, The structure of 2,6-di-tert-butylphenol–argon by rotational spectroscopy, Molecules 28 (24) (2023) 8111.
[13] W. Li, A. Maris, S. Melandri, A. Lesarri, L. Evangelisti, Molecular structure and internal dynamics of the antioxidant 2, 6-di-tert-butylphenol, Journal of Molecular Structure 1296 (2024) 136910.
[14] W. Li, D. Heras, A. Maris, S. Melandri, A. Lesarri, L. Evangelisti, A rotational study of 2-tert-butylphenol and Its 1: 1 argon complex, ChemPhysChem (2024) e202400089.
[15] J.L. Neill, L. Evangelisti, B.H. Pate, Analysis of isomeric mixtures by molecular rotational resonance spectroscopy, Analytical Science Advances 4 (5–6) (2023) 204–219.
[16] D.D. Beusen, E.B. Shands, S.F. Karasek, G.R. Marshall, R.A. Dammkoehler, Systematic search in conformational analysis, Journal of Molecular Structure: THEOCHEM 370 (2–3) (1996) 157–171.
[17] M.J. Frisch, G.W. Trucks, H.B. Schlegel, G.E. Scuseria, M.A. Robb, J.R. Cheeseman, G. Scalmani, V. Barone, G.A. Petersson, H. Nakatsuji, X. Li, M. Caricato, A. V. Marenich, J. Bloino, B.G. Janesko, R. Gomperts, B. Mennucci, H.P. Hratchian, J. V. Ortiz, A.F. Izmaylov, J.L. Sonnenberg, D. Williams-Young, F. Ding, F. Lipparini, F. Egidi, J. Goings, B. Peng, A. Petrone, T. Henderson, D. Ranasinghe, V. G. Zakrzewski, J. Gao, N. Rega, G. Zheng, W. Liang, M. Hada, M. Ehara, K. Toyota, R. Fukuda, J. Hasegawa, M. Ishida, T. Nakajima, Y. Honda, O. Kitao, H. Nakai, T. Vreven, K. Throssell, J.A. Montgomery Jr., J.E. Peralta, F. Ogliaro, M. J. Bearpark, J.J. Heyd, E.N. Brothers, K.N. Kudin, V.N. Staroverov, T.A. Keith, R. Kobayashi, J. Normand, K. Raghavachari, A.P. Rendell, J.C. Burant, S.S. Iyengar, J. Tomasi, M. Cossi, J.M. Millam, M. Klene, C. Adamo, R. Cammi, J.W. Ochterski, R.L. Martin, K. Morokuma, O. Farkas, J.B. Foresman, D.J. Fox, Gaussian 16 Revision C. 01. 2016, Gaussian Inc., Wallingford CT, 2016, p. 421.
[18] A.D. Beck, Density-functional thermochemistry. III. The role of exact exchange, Journal of Chemical Physics 98 (7) (1993) 5648.
[19] S. Grimme, S. Ehrlich, L. Goerigk, Effect of the damping function in dispersion corrected density functional theory, Journal of Computational Chemistry 32 (7) (2011) 1456–1465.
[20] F. Weigend, R. Ahlrichs, Balanced basis sets of split valence, triple zeta valence and quadruple zeta valence quality for H to Rn: Design and assessment of accuracy, Physical Chemistry Chemical Physics 7 (18) (2005) 3297–3305.
[21] M. Juanes, I. Usabiaga, I. León, L. Evangelisti, J.A. Fernández, A. Lesarri, The six isomers of the cyclohexanol dimer: A delicate test for dispersion models, Angewandte Chemie International Edition 59 (33) (2020) 14081–14085.
[22] C. Calabrese, W. Li, G. Prampolini, L. Evangelisti, I. Uriarte, I. Cacelli, S. Melandri, E.J. Cocinero, A general treatment to study molecular complexes stabilized by hydrogen-, halogen-, and carbon-bond networks: Experiment and theory of $(CH_2F_2)_n\cdots(H_2O)_m$, Angewandte Chemie International Edition 58 (25) (2019) 8437–8442.
[23] G.G. Brown, B.C. Dian, K.O. Douglass, S.M. Geyer, S.T. Shipman, B.H. Pate, A broadband Fourier transform microwave spectrometer based on chirped pulse excitation, Review of Scientific Instruments 79 (5) (2008).
[24] J.K. Watson, J.R. Durig (Eds.), Vibrational Spectra and Structure, Elsevier, Amsterdam, 1977, pp. 1–89.
[25] H.M. Pickett, The fitting and prediction of vibration-rotation spectra with spin interactions, Journal of Molecular Spectroscopy 148 (2) (1991) 371–377.
[26] R.S. Ruoff, T.D. Klots, T. Emilsson, H.S. Gutowsky, Relaxation of conformers and isomers in seeded supersonic jets of inert gases, The Journal of Chemical Physics 93 (5) (1990) 3142–3150.
[27] K. Mayer, C. West, F.E. Marshall, G. Sedo, G.S. Grubbs, L. Evangelisti, B.H. Pate, Accuracy of quantum chemistry structures of chiral tag complexes and the assignment of absolute configuration, Physical Chemistry Chemical Physics 24 (45) (2022) 27705–27721.
[28] J. Kraitchman, Determination of molecular structure from microwave spectroscopic data, American Journal of Physics 21 (1) (1953) 17–24.
[29] L. Evangelisti, C. Perez, N.A. Seifert, B.H. Pate, M. Dehghany, N. Moazzen-Ahmadi, A.R.W. McKellar, Theory vs. experiment for molecular clusters: Spectra of OCS trimers and tetramers, The Journal of Chemical Physics 142 (10) (2015) 104309.

[30] A.H. Cheng, A. Lo, S. Miret, B.H. Pate, A. Aspuru-Guzik, Determining 3D structure from molecular formula and isotopologue rotational spectra in natural abundance with reflection-equivariant diffusion, The Journal of Chemical Physics 160 (12) (2024).
[31] L.S. Vedula, G. Brannigan, N.J. Economou, J. Xi, M.A. Hall, R. Liu, M.J. Rossi, W. P. Dailey, K.C. Grasty, M.L. Klein, R.G. Eckenhoff, A unitary anesthetic binding site at high resolution, Journal of Biological Chemistry 284 (36) (2009) 24176–24184.
[32] R. Meyer, Trigonometric interpolation method for one-dimensional quantum-mechanical problems, The Journal of Chemical Physics 52 (4) (1970) 2053–2059.
[33] R. Meyer, Flexible models for intramolecular motion, a versatile treatment and its application to glyoxal, Journal of Molecular Spectroscopy 76 (1–3) (1979) 266–300.
[34] L. Paoloni, A. Maris, Interplay of rotational and pseudorotational motions in flexible cyclic molecules, The Journal of Physical Chemistry A 125 (19) (2021) 4098–4113.
[35] S. Albert, P. Lerch, R. Prentner, M. Quack, Tunneling and tunneling switching dynamics in phenol and its isotopomers from high-resolution FTIR spectroscopy with synchrotron radiation, Angewandte Chemie International Edition 52 (1) (2013) 346–349.